Inorganic Chemistry

pubs.acs.org/IC

Featured Article

Conjugated-Polypyridine-Derivative-Derived Semiconductive Iodoplumbates with Tunable Architectures and Efficient Visible-Light-Induced Photocatalytic Property

Chen Li, Kui Wang, Xin-Yu Li, Xiao-Fan Jiang, Qi Wei, Jin-Hua Li,* and Guo-Ming Wang

Cite This: *Inorg. Chem.* 2021, 60, 2105−2111

Read Online

ACCESS | Metrics & More | Article Recommendations | Supporting Information

ABSTRACT: By mediation of the pH values, three novel inorganic−organic iodoplumbate hybrids, $[Me_3TPT][Pb_3I_9]$ [**1**; Me_3TPT = trimethyl-2,4,6-tris(4-pyridyl)-1,3,5-triazine], $[Me_3TPT]_2[Pb_9I_{24}]$ (**2**), and $[Me_3TPT]_2[Pb_{19}I_{44}]$ (**3**), have been achieved under solvothermal conditions. The large conjugated in situ N-alkylation polypyridine derivatives act as structure-directing agents and electron acceptors, making the materials feature adjustable structural variations with 0D, 1D, and 2D structures and a potential semiconductive performance with narrow energy gaps (1.72, 1.80, and 1.78 eV for **1**−**3**, respectively), which result in their efficient photocatalytic activity under visible-light irradiation. Theoretical calculation reveals that the conjugated organic moieties greatly contribute to the conduction band, leading to narrow band gaps. It is expected that the work will contribute to the exploitation of novel semiconducting halometallates by employing conjugated organic species as structure-directing agents.

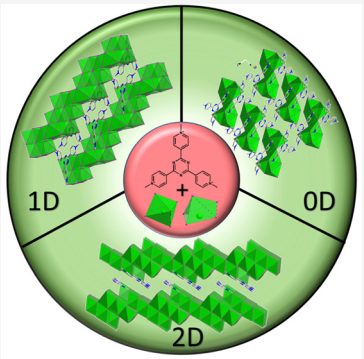

INTRODUCTION

Halometallate hybrids as functional materials, taking advantage of organic and inorganic constituents, have received great interest because of their potential applications in various areas such as semiconductors, photoluminescence, photo/thermochroism, and dielectric materials.[1−15] Structurally, the halide atoms (Cl^-, Br^-, or I^-) can serve as linkers from terminal to μ_2 and up to μ_8 bridging. The combination of different metal atoms with halide ions gives rise to a large amount of haloplumbate anions. The formation of these haloplumbate anions is kinetically controlled and highly sensitive to reaction parameters. Subtle changes may lead to their diverse aggregates. Therefore, numerous desirable structures based on diverse anions with captivating physicochemical properties were achieved. For instance, Zhang, Fu, and co-workers reported a series of iodocuprates(I) and bromocuprates(I) that feature interesting photochromic or thermochromic phenomena.[16−19] Lei, Yue, and co-workers systematically investigated iodoargentate and iodocuprate(I) hybrids based on the transition-metal complexes that exhibit photocatalytic or photoelectric properties.[20−24]

Recently, as an important subclass of halometallate hybrids, haloplumbates have received enormous interest because of their important physicochemical properties, which are favorable for optoelectronic and photocatalytic applications.[6,12,25−29] However, the materials still face a great challenge: they are underpowered to meet the requirements for tunable band gaps, which limits their widespread applications. The template, as a crucial factor in the formation of compounds, not only plays a "structure-directing" role in controlling the complexity and dimensions of the resultant products but also could modulate the electronic band and further regulate their photoelectric properties. Structurally, organic templates exhibit different size, shape, and flexible spatial configurations and distribution of the charges, providing rich methodologies and more potential to direct diverse desirable materials. Therefore, employment of function-enhanced organic templates was proved to be an effective strategy for design and explore novel functional hybrids. Besides, some functional organic species with electron-deficient characteristics have been introduced into halides to design and develop donor−acceptor hybrids.[11,30,31] The electron-deficient organic species exhibit strong electron-accepting abilities, which can regulate the electronic structures to further affect the physicochemical properties of the materials. The large conjugated organic species are beneficial to accomplishing electron delocalization, which offers a great possibility for modulation or improvement of the electronic and optical properties of the designed halometallates.

Our research on the systematic exploration of halometallate hybrids employing large conjugated polypyridine groups as templates has made some progress.[14,32−34] These results reveal

Received: December 15, 2020
Published: January 28, 2021

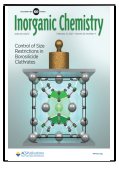

https://dx.doi.org/10.1021/acs.inorgchem.0c03665
Inorg. Chem. 2021, 60, 2105−2111

that the conjugated in situ templates can effectively lower the energy gap and accordingly increase the absorption of visible light. Here, to investigate the influence of different large conjugated organic templates on the crystal and band structures on iodoplumbates, by using conjugated in situ N-alkylation 2,4,6-tris(4-pyridyl)-1,3,5-triazine (TPT) derivatives as templates and mediating the pH values, three novel iodoplumbate hybrids, $[Me_3TPT][Pb_3I_9]$ (**1**) $[Me_3TPT]_2[Pb_9I_{24}]$ (**2**), and $[Me_3TPT]_2[Pb_{19}I_{44}]$ (**3**), were achieved. They exhibit adjustable structural variations with 0D, 1D, and 2D structures, respectively. UV−vis spectral analyses reveal that the compounds are potential semiconductive materials with narrow energy gaps, further resulting in the efficient photocatalytic activity under visible-light irradiation. Theoretical calculation reveals that the conjugated organic moieties greatly contribute to the conduction band, leading to the narrow band gaps of the materials.

EXPERIMENTAL SECTION

Materials and Methods. The chemicals employed in the work were of commercially available analytical grade and were used directly without further purification. Powder X-ray diffraction (PXRD) patterns were carried out on a Bruker D8 FOCUS diffractometer with Cu Kα radiation (λ = 1.540598 Å; 2θ = 5−50°). Elemental analysis was performed on a PerkinElmer 240C analyzer. IR spectra were measured on a TENSOR 27 (Bruker) Fourier transform infrared spectrometer. UV−vis spectra were measured performed on a PerkinElmer Lamda-950 spectrophotometer. A $BaSO_4$ plate was used as the standard. Thermogravimetric analysis (TGA) data were collected in an air atmosphere using a Mettler TGA/SDTA 851 thermal analyzer.

Synthesis of $[Me_3TPT][Pb_3I_9]$ (1). A mixture of $Pb(NO_3)_2$ (0.0665 g, 0.2 mmol), TPT (0.0223 g, 0.065 mmol), NaI (0.0299 g, 0.2 mmol), HI (0.15 mL, 45%), and CH_3OH (5.0 mL) was sealed in a Teflon autoclave (23.0 mL) with a pH value of 0.45. Then, the mixture was heated to 160 °C for 7 days. Red crystals were synthesized (74.3% yield based on TPT). Elem anal. Calcd for $C_{21}H_{21}I_9N_6Pb_3$ (fw 2121.17): C, 11.89; H, 0.99; N, 3.96. Found: C, 12.01; H, 1.08; N, 3.88. IR (cm^{-1}): 3469(s), 3050(m), 2915(w), 1612(s), 1515(s), 1370(m), 1310(w), 804(w) (Figure S1).

Synthesis of $[Me_3TPT]_2[Pb_9I_{24}]$ (2). A mixture of $Pb(NO_3)_2$ (0.0992 g, 0.30 mmol), TPT (0.0223 g, 0.065 mmol), NaI (0.0300 g, 0.2 mmol), HI (0.2 mL, 45%), and CH_3OH (5.0 mL) was sealed in a Teflon autoclave (23.0 mL). The pH value of the mixture was 0.24. Then, it was heated at 160 °C (87.8% yield based on TPT). Elem anal. Calcd for $C_{42}H_{42}I_{24}N_{12}Pb_9$ (fw 5625.37): C, 8.96; H, 0.75; N, 2.98. Found: C, 9.01; H, 0.91; N, 3.09. IR (cm^{-1}): 3490(s), 3048(m), 2910(w), 1620(s), 1520(s), 1437(m), 1375(m), 1236(w), 1139(w), 804(s) (Figure S1).

Synthesis of $[Me_3TPT]_2[Pb_{19}I_{44}]$ (3). A mixture of $Pb(NO_3)_2$ (0.1994 g, 0.6 mmol), TPT (0.0223 g, 0.065 mmol), NaI (0.0452 g, 0.3 mmol), HI (0.4 mL, 45%), and CH_3OH (5.0 mL) was sealed in a Teflon autoclave (23.0 mL) with a pH value of 0.16. The mixture were heated at 160 °C for 7 days. Red crystals of **3** were obtained (68.8% yield based on TPT). Elem anal. Calcd for $C_{42}H_{42}I_{44}N_{12}Pb_{19}$ (fw 10235.09): C, 4.92; N, 1.64. Found: C, 5.03; N, 1.49. IR (cm^{-1}): 3490(s), 3055(m), 2910(w), 1620(s), 1520(s), 1370(s), 1270(w), 1150(w), 800(m) (Figure S1).

Structure Determination. Data collection for single-crystal structures was performed on a XtaLAB-mini diffractometer with Mo Kα radiation (λ = 0.71073 Å, 293 K). Absorption corrections based on the Multiscan method[35] were applied. All of the structures were solved by direct methods and refined by the *SHELXTL* system.[36−38] The non-H atoms were refined with anisotropic thermal parameters. Relevant crystallographic data are listed in Table 1. CCDC 2047292 (**1**), 2047293 (**2**), and 2047294 (**3**) contain the supplementary crystallographic data for the paper.

Table 1. Summary of the Crystal Data and Structural Refinements for Compounds 1−3

	1	2	3
formula	$C_{21}H_{21}N_6Pb_3I_9$	$C_{42}H_{42}N_{12}Pb_9I_{24}$	$C_{42}H_{42}N_{12}Pb_{19}I_{44}$
M_r (g mol^{-1})	2121.11	5625.19	10235.09
space group	$P\bar{1}$	$P2_1/c$	$P\bar{1}$
cryst syst	triclinic	monoclinic	triclinic
a (Å)	10.7557(7)	12.6175(14)	15.3278(7)
b (Å)	12.8460(9)	12.0213(3)	17.8002(8)
c (Å)	16.2308(11)	32.523(3)	17.8320(7)
α (deg)	100.506(6)	90(18)	112.823(4)
β (deg)	93.892(5)	91.495(6)	97.691(4)
γ (deg)	105.052(6)	90(2)	114.875(5)
V (Å^3)	2113.6(2)	4931.4(10)	3803.1(3)
Z	2	2	1
F (000)	1824	4776	4268
D_c (g cm^{-3})	3.333	3.788	4.469
μ (mm^{-1})	18.513	22.848	110.250
R_{int}	0.0438	0.1529	0.0645
collected reflns	10971	34237	27606
unique reflns	7445	8656	14273
GOF on F^2	0.957	1.125	0.0645
R_1, wR_2 [$I > 2\sigma(I)$][a]	0.0479, 0.0988	0.0754, 0.1796	0.0677, 0.1784
R_1, wR_2 (all data)[a]	0.0932, 0.1138	0.0935, 0.1933	0.0850, 0.1990

[a] $R_1 = \sum||F_o| - |F_c||/\sum|F_o|$. $wR_2 = [\sum w(F_o^2 - F_c^2)^2/\sum w(F_o^2)^2]^{1/2}$.

Photocatalytic Experiments. Congo red (CR) was selected to assess the photocatalytic activity. A total of 50 mg of samples was added to 50 mL of an ethanol solution (1×10^{-5} mol L^{-1}) in a quartz tube. The suspension was stirred in the dark for 50 min in order to reach absorption−desorption equilibrium. Then, it was exposed in a xenon lamp (500 W) fitted with a 420 nm cutoff filter at room temperature. A total of 2.0 mL of the test mixture was taken out every 3 min. The solid samples were separated from the suspensions by centrifugation. The absorption spectra of the resulting supernatant fluid were measured on a TU-1901 UV−vis spectrophotometer.

Computational Methods. Electronic structure calculations were performed using the density functional theory (DFT) method embedded in the *CASTEP* code in the *Material Studio* package.[39] The local density approximation (LDA) was adopted, with the spin-polarized effect being considered. The plane-wave energy cutoff was set at 350.0 eV. Numerical integration of the Brillouin zone was performed by a 2 × 2 × 2 Monkhorst−Pack *k*-point sampler.

RESULTS AND DISCUSSION

Syntheses. By systematic regulation of the pH values, three new iodoplumbates, i.e., the isolated **1**, the ribbonlike **2**, and the layered **3**, were successfully synthesized by a solvothermal treatment with the same starting material. IR, elemental analysis, and PXRD determination were used to verify the phase purity of **1**−**3** (Figures S1 and S2). They were all synthesized under acidic conditions. The starting material of TPT molecules underwent in situ N-alkylation reaction. TPT was reacted with alcohols and HI to give rise to methylated cations, which played an important role in the self-assembly process of the obtained products (Schemes 1 and S1). It is noteworthy that the one-step in situ synthesis is more convenient and efficient compared with the conventional N-alkylation synthesis. Moreover, it also provides more possibilities for the generation of new organic templates. Actually, although many organic bases were used to guide the

https://dx.doi.org/10.1021/acs.inorgchem.0c03665
Inorg. Chem. 2021, 60, 2105−2111

Scheme 1. In Situ N-Methylation of TPT

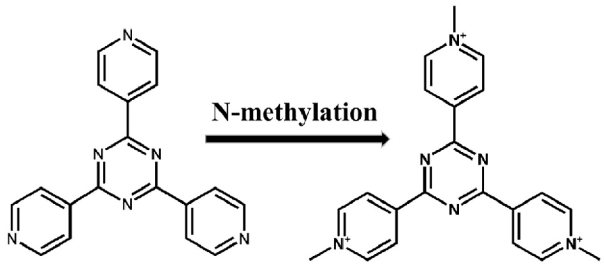

halometallate hybrids, reports on novel structure-directing agents (SDAs) generated in situ are still rare.

Moreover, the syntheses employed $Pb(NO_3)_2$ as the lead(II) source, NaI and HI as the source of the I anion, and HI as the pH mediator. On the basis of the results from the experiments, it was found that the amounts of HI employed were important for the obtained products. When the volumes of HI were 0.15, 0.20, and 0.40 mL with a solvent of 5.0 mL of CH_3OH, the isolated **1**, the ribbonlike **2**, and the layered **3** were obtained, respectively. Structural evolution from the 0D, 1D, to 2D structures showed the important influence of acidity on the structure formation. Presumably, increasing the acidity may be beneficial to the formation of high-dimensional structures. Regretfully, increasing the volume of HI to more than 0.40 mL for the 3D structure failed. In total, this work revealed that subtle changes in the solvothermal synthetic progress can influence the generation of compounds and regulating the pH values is an effective way of generating novel halides under solvothermal conditions.

Crystal Structures. Single-crystal X-ray diffraction characterizations revealed that **1** crystallizes in the space group $P\bar{1}$ (Table 1 and S1). The asymmetric unit includes three crystallographically independent Pb^{2+} ions, nine I^- ions, and one $[Me_3TPT]^{3+}$ cation. In **1**, Pb^{2+} ions show two coordination modes: Pb(1) and Pb(2) ions are coordinated by six I^- to yield PbI_6 distorted octahedra with Pb−I bond lengths in the range of 2.985(1)−3.452(1) Å, and Pb(3) is five-coordinate in a PbI_5 distorted tetragonal pyramid with Pb−I lengths ranging from 2.985(1) to 3.452(1) Å (Figure 1a). The distorted octahedra and tetragonal pyramid are linked by face-sharing, generating a trimeric Pb_3I_{10} ($\{Pb_3\}$) cluster as the secondary building unit (SBU) of **1**. Two $\{Pb_3\}$ clusters link together via edge-sharing to form the isolated structural unit Pb_6I_{18}. The $[Me_3TPT]^{3+}$ cations as counterions occupy the space between the Pb_6I_{18} units (Figure 1b).

2 crystallizes in the space group $P2_1/c$ (Table 1 and S2), and the asymmetric unit comprises 5 unique Pb^{2+} ions, 12 I^- ions, and 1 $[Me_3TPT]^{3+}$ cation. Notably, different from the two-coordinate geometries of the Pb^{2+} ions in **1**, all of the Pb^{2+} ions are six-coordinate with $[PbI_6]$ octahedral geometries, and the Pb−I bond lengths are in the range of 2.866(4)−3.553(4) Å. The linkage of nine PbI_6 octahedra results in a unique Pb_9I_{30} ($\{Pb_9\}$) cluster as the SBU of **2** (Figure 2a). The $\{Pb_9\}$) SBUs are further connected with each other by edge-sharing, generating a 1D $[Pb_9I_{24}]^{6-}$ ribbonlike structure (Figure 2b). The coupled $[Me_3TPT]^{3+}$ cations compensate for the negative charges of the ribbonlike structure and precisely accommodate the space between the anionic ribbons (Figure 2c).

Compound **3** belongs to the space group $P\bar{1}$ (Tables 1 and S3). In the asymmetric unit, there are 10 crystallographically distinguished Pb^{2+} ions, 22 I^- ions, and 1 $[Me_3TPT]^{3+}$ cations.

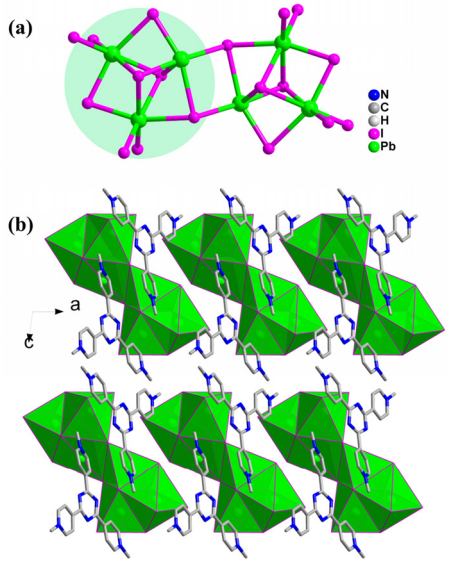

Figure 1. (a) View of the $\{Pb_3\}$ cluster in **1**. (b) Polyhedral view of the 3D structure.

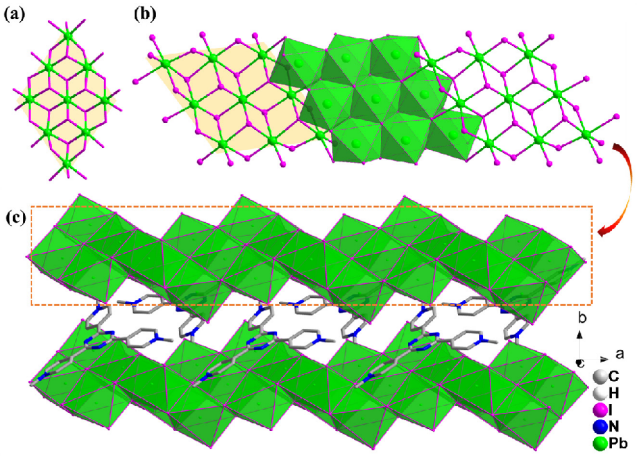

Figure 2. (a) View of the $\{Pb_9\}$ cluster in **2**. (b) View of the 1D $[Pb_9I_{24}]^{6-}$ ribbonlike structure. (c) Polyhedral view of the 3D structure.

Similar to **2**, all 10 Pb atoms exhibit distorted PbI_6 octahedral coordinate geometries with bond lengths in the range from 2.937(4) to 3.564(4) Å. Notably, one of the most striking features of **3** is the two types of SBUs: $Pb(1)I_6$, $Pb(2)I_6$, $Pb(3)I_6$, $Pb(4)I_6$, and $Pb(5)I_6$ octahedra are alternately arranged via edge-sharing in a Pb_9I_{30} ($\{Pb_9\}$) cluster (Figure 3a), which exhibits the same arrangement as that of the $\{Pb_9\}$ SBU in **2**. Another five unique Pb atoms are six-coordinate and further linked with each other, giving rise to the second SBU of **3**, a rare $Pb_{10}I_{36}$ ($\{Pb_{10}\}$) cluster (Figure 3a). Interestingly, the arrangement of $\{Pb_{10}\}$ SBUs via edge-sharing generates a ribbon structure. The $\{Pb_9\}$ SBUs as the linkers connect the $\{Pb_{10}\}$-based ribbon structures into an anionic 2D $[Pb_{19}I_{44}]^{6-}$ layer (Figure 3b). Furthermore, the single layers are stacked in parallel and connected via the weak C−H···I hydrogen bonds, leading to a 3D supramolecular architecture (Figure 3c).

Optical Properties. The IR spectra are shown in Figure S1. N-Alkylation of TPT can be further confirmed by the characteristic peaks of the $-CH_3$ units in the IR spectra. The bands at 3055−2900 and 1375 cm^{-1} are directly related to the

https://dx.doi.org/10.1021/acs.inorgchem.0c03665
Inorg. Chem. 2021, 60, 2105−2111

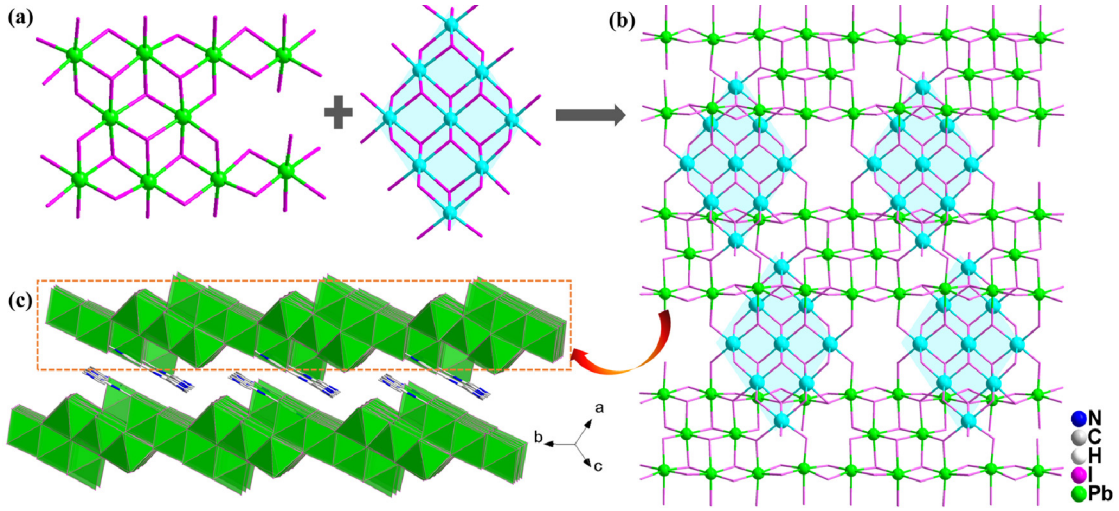

Figure 3. (a) View of the $\{Pb_{10}\}$ and $\{Pb_9\}$ clusters in **3**. (b) View of the $[Pb_{19}I_{44}]^{6-}$ layer. (c) Polyhedral view of the 3D structure. Color code: Pb, green and cyan.

stretching and in-plane bending vibrations of the C−H bonds in the $-CH_3$ units, respectively, suggesting that the TPT units have been methylated and further directing the corresponding structures. All the three spectra exhibit similar vibrational absorptions and are in accordance with the structural analyses.

The UV−vis absorption spectra reveal that the band gaps for compounds **1**−**3** are 1.72, 1.80, and 1.78 eV (Figure 4),

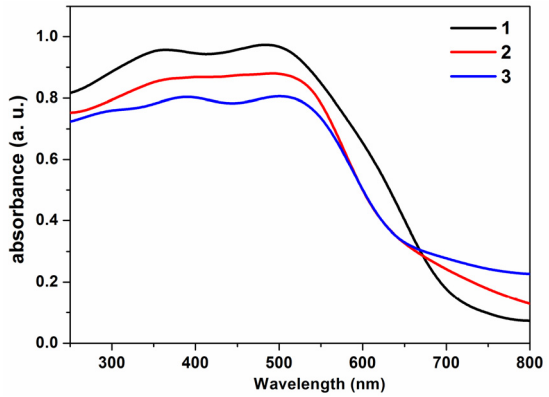

Figure 4. Solid-state UV−vis spectra of compounds **1**−**3**.

respectively, which suggests that they are potential semiconducting hybrid materials. Notably, the materials possess narrower band gaps and represent red shifts relative to the initial reactants, i.e., $Pb(NO_3)_2$ (3.96 eV) and NaI (3.24 eV), owing to the contribution of the conjugated organic units to the conduction bands (Figure S3). Moreover, it is worth noting that the band-gap values are comparable to those of other conjugated organic-template-based halometallates, such as (*N*-methylpyrrolidinium)$_3[Sb_2Br_9]$ (2.76 eV),[4] (4-methylpiperidinium)$_3[Bi_2I_9]$ (2.02 eV),[40] (isopropylviologen)$[Pb_2I_6]$ (1.86 eV),[27] and $[Me_2(bpanth)][Pb_4I_{10}]$ (bpanth = 9, 10-bis(4-pyridyl)anthracene; 2.06 eV),[41] which feature the properties of semiconducting materials.

Photocatalytic Properties. Encouraged by the narrow band gaps (1.72, 1.80, and 1.78 eV for **1**−**3**, respectively), the visible-light-driven photocatalytic behavior was investigated. Compound **3** was selected as the representation, and the photocatalytic activity was assessed by degradation of the CR organic pollutant under visible-light irradiation at room temperature. As shown in Figure 5, it is clear that CR self-

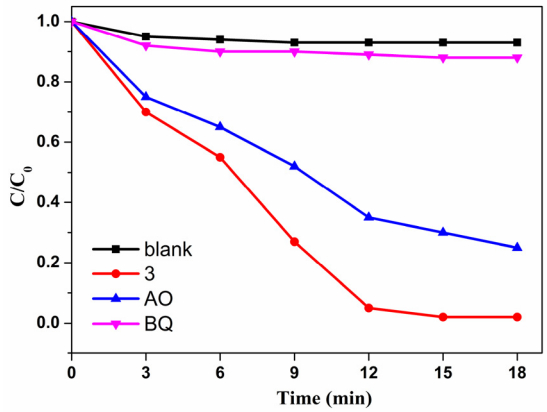

Figure 5. Photocatalytic degradation of CR of compound **3** under visible-light irradiation.

photodegradation in the absence of catalysts shows no observable decrease in the concentration. Under visible-light irradiation, when as-prepared **3** was added to the dye solutions, the color of the solution became lighter and became colorless within 15 min. Correspondingly, the concentration decreased with the irradiation time, which suggests that the samples can effectively work for degradation of the CR dye. Moreover, the reaction rate constant (k) was evaluated following a pseudo-first-order kinetic model, $\ln(C_0/C) = kt$ (C_0, initial concentration; C, residual concentration) and its value estimated to be about 0.240 min^{-1} (Figure S4). In order to get a better understanding of the photocatalytic activity, radical trapping tests were carried out to detect the main reactive species in the process of degradation. Ammonium oxalate and benzoquinone (BQ) were chosen as trapping agents for the hole (h^+) and superoxide ($\dot{O}_2^-$) radicals, respectively.[22,23,42−46] As a result, the catalytic efficiency was dramatically suppressed when BQ was introduced, suggesting that $\dot{O}_2^-$ is the main active species for the CR degradation.

To further investigate the relationships between the structure and properties, electronic structure calculation

https://dx.doi.org/10.1021/acs.inorgchem.0c03665
Inorg. Chem. 2021, 60, 2105−2111

based on DFT was performed. As shown in Figure 6, the top of the valence band ranging from ~4.0 to 0 eV is mainly

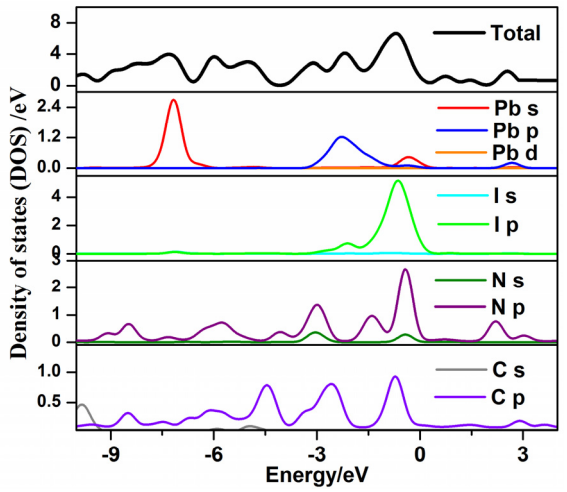

Figure 6. Total and partial density of states of compound **3**.

constructed from I 5p, Pb 6p, N 2p, and C 2p states, while the bottom of the conduction band originates primarily from N 2p with small amounts of C 2p and Pb 6p states. Therefore, it can be found that the conjugated $[Me_3TPT]^{3+}$ cations mainly contribute to the conduction band, decreasing the energy position and resulting in a narrow band gap. It is reasonable to deduce that the optical absorptions may be mainly attributed to charge transitions from the inorganic networks to the conjugated $[Me_3TPT]^{3+}$ organic moieties.

Furthermore, the three compounds in this work, as well as the reported halometallates templated by conjugated organic cations, such as $[Pb_3CuI_{10}(Me_3TPT)]$,[32] $[(Me)_3TPT]_2[Cu_{12}I_{18}]$,[14] $[Me_2(bpanth)][Pb_4I_{10}]$,[41] $[(Me)_2$-2,2′-bipy$][Cu_8I_{10}]$,[22] [*N*-ethyl-4-cyanopyridinium$][Ag_2I_3]$,[47] $[Me_3TPB][Cu_5I_8]$ [TPB = 1,3,5-tris(4-pyridyl)benzene],[48] [*N*-benzylpyridinium$]_2[Cu_6I_8]$,[19] and $[Me_3(4$-TPT$)]_4[Ag_6I_{18}]$,[34] all possess narrow band gaps. Combined with the results of theoretical calculations, it is speculated that the large conjugated organic cations can greatly contribute to the conduction band and regulate the electronic band structures, and introducing the large conjugated organic cations as templates in halometallates may be an effective way of developing semiconductive hybrids.

CONCLUSIONS

In summary, by regulation of the pH values, three novel iodoplumbate hybrids were achieved based on the large conjugated polypyridine cations by an efficient in situ one-step reaction. They exhibit adjustable structural variations with 0D, 1D, and 2D structures based on diverse SBUs. The materials possess narrow band gaps and exhibit efficient photocatalytic performances in the visible-light-driven degradation of an organic dye. Theoretical calculation shows that the conjugated TPT species contributed to the semiconducting behavior, further generating excellent visible-light-driven photocatalytic activity. The work is anticipated to provide an opportunity to design and develop novel halometallate hybrids with excellent photosensitive properties.

ASSOCIATED CONTENT

Supporting Information

The Supporting Information is available free of charge at https://pubs.acs.org/doi/10.1021/acs.inorgchem.0c03665.

Atomic coordinates and equivalent isotropic displacement parameters of **1**−**3**, detailed in situ N-methylation of TPT, simulated and measured PXRD patterns, and IR and absorption spectra, linear relationship of $\ln(C_0/C)$, and TGA curve (PDF)

Accession Codes

CCDC 2047292−2047294 contain the supplementary crystallographic data for this paper. These data can be obtained free of charge via www.ccdc.cam.ac.uk/data_request/cif, or by emailing data_request@ccdc.cam.ac.uk, or by contacting The Cambridge Crystallographic Data Centre, 12 Union Road, Cambridge CB2 1EZ, UK; fax: +44 1223 336033.

AUTHOR INFORMATION

Corresponding Author

Jin-Hua Li − *College of Chemistry and Chemical Engineering, Qingdao University, Qingdao, Shandong 266071, P. R. China;* orcid.org/0000-0001-7352-9333; Email: jinhuali1978@163.com

Authors

Chen Li − *College of Chemistry and Chemical Engineering, Qingdao University, Qingdao, Shandong 266071, P. R. China*

Kui Wang − *College of Chemistry and Chemical Engineering, Qingdao University, Qingdao, Shandong 266071, P. R. China*

Xin-Yu Li − *College of Chemistry and Chemical Engineering, Qingdao University, Qingdao, Shandong 266071, P. R. China*

Xiao-Fan Jiang − *College of Chemistry and Chemical Engineering, Qingdao University, Qingdao, Shandong 266071, P. R. China*

Qi Wei − *College of Chemistry and Chemical Engineering, Qingdao University, Qingdao, Shandong 266071, P. R. China;* orcid.org/0000-0003-0049-308X

Guo-Ming Wang − *College of Chemistry and Chemical Engineering, Qingdao University, Qingdao, Shandong 266071, P. R. China;* orcid.org/0000-0003-0156-904X

Complete contact information is available at: https://pubs.acs.org/10.1021/acs.inorgchem.0c03665

Notes

The authors declare no competing financial interest.

ACKNOWLEDGMENTS

This work was supported by grants from the National Natural Science Foundation of China (Grants 22071125, 22071126, and 22001142), the Key Research and Development Project of Shandong Province (Grant 2019GGX102006), the Natural Science Foundation of Shandong Province (Grant ZR2018BB003), and the China Postdoctoral Science Foundation (Grant 2019M652308).

REFERENCES

(1) Yu, T.-L.; Guo, Y.-M.; Wu, G.-X.; Yang, X.-F.; Xue, M.; Fu, Y.-L.; Wang, M.-S. Recent progress of d10 iodoargentate(I)/iodocuprate(I)

hybrids: Structural diversity, directed synthesis, and photochromic/thermochromic properties. *Coord. Chem. Rev.* **2019**, *397*, 91−111.
(2) Peng, R.; Li, M.; Li, D. Copper(I) halides: A versatile family in coordination chemistry and crystal engineering. *Coord. Chem. Rev.* **2010**, *254* (1−2), 1−18.
(3) Mao, L.; Guo, P.; Kepenekian, M.; Hadar, I.; Katan, C.; Even, J.; Schaller, R. D.; Stoumpos, C. C.; Kanatzidis, M. G. Structural Diversity in White-Light-Emitting Hybrid Lead Bromide Perovskites. *J. Am. Chem. Soc.* **2018**, *140* (40), 13078−13088.
(4) Sun, Z.; Zeb, A.; Liu, S.; Ji, C.; Khan, T.; Li, L.; Hong, M.; Luo, J. Exploring a Lead-free Semiconducting Hybrid Ferroelectric with a Zero-Dimensional Perovskite-like Structure. *Angew. Chem., Int. Ed.* **2016**, *55* (39), 11854−11858.
(5) Sun, C.; Xu, G.; Jiang, X. M.; Wang, G. E.; Guo, P. Y.; Wang, M. S.; Guo, G. C. Design Strategy for Improving Optical and Electrical Properties and Stability of Lead-Halide Semiconductors. *J. Am. Chem. Soc.* **2018**, *140* (8), 2805−2811.
(6) Wang, G.-E.; Yao, M.-S.; Cai, M.-L.; Xiu, J.-W.; Li, Y.-Z.; Xu, G.; Guo, G.-C. Constructing semiconductive crystalline microporous materials by Coulomb interactions. *J. Mater. Chem. A* **2017**, *5* (35), 18409−18413.
(7) Khan, A.; Han, S.; Liu, X.; Tao, K.; Dey, D.; Luo, J.; Sun, Z. A new antimony-based organic−inorganic hybrid absorber with photoconductive response. *Inorg. Chem. Front.* **2018**, *5* (12), 3028−3032.
(8) Yue, C.-Y.; Sun, H.-X.; Liu, Q.-X.; Wang, X.-M.; Yuan, Z.-S.; Wang, J.; Wu, J.-H.; Hu, B.; Lei, X.-W. Organic cation directed hybrid lead halides of zero-dimensional to two-dimensional structures with tunable photoluminescence properties. *Inorg. Chem. Front.* **2019**, *6* (10), 2709−2717.
(9) Li, X.; Ha Do, T. T.; Granados Del Aguila, A.; Huang, Y.; Chen, W.; Li, Y.; Ganguly, R.; Morris, S.; Xiong, Q.; Li, D. S.; Zhang, Q. Two-Dimensional and Emission-Tunable: An Unusual Perovskite Constructed from Lindqvist-Type $[Pb_6Br_{19}]^{7-}$ Nanoclusters. *Inorg. Chem.* **2018**, *57* (22), 14035−14038.
(10) Hao, P.; Zhang, L.; Shen, J.; Fu, Y. Structural and photochromic modulation of dimethylbenzotriazolium iodoargentate hybrid materials. *Dyes Pigm.* **2018**, *153*, 284−290.
(11) Wang, Z. P.; Wang, J. Y.; Li, J. R.; Feng, M. L.; Zou, G. D.; Huang, X. Y. $[Bmim]_2SbCl_5$: a main group metal-containing ionic liquid exhibiting tunable photoluminescence and white-light emission. *Chem. Commun.* **2015**, *51* (15), 3094−7.
(12) Zhao, L.-M.; Zhang, W.-T.; Song, K.-Y.; Wu, Q.-Q.; Li, Y.; Li, H.-H.; Chen, Z.-R. Lead-carboxylate/polyiodide hybrids constructed from halogen bonding and asymmetric viologen: structures, visible-light-driven photocatalytic properties and enhanced photocurrent responses. *CrystEngComm* **2018**, *20* (16), 2245−2252.
(13) Liu, M. M.; Hou, J. J.; Qi, Z. K.; Duan, L. N.; Ji, W. J.; Han, C. Y.; Zhang, X. M. Tuning of valence States, bonding types, hierarchical structures, and physical properties in copper/halide/isonicotinate system. *Inorg. Chem.* **2014**, *53* (8), 4130−4143.
(14) Sun, A.-H.; Han, S.-D.; Pan, J.; Li, J.-H.; Wang, G.-M.; Wang, Z.-H. 3D Inorganic Cuprous Iodide Open-Framework Templated by In Situ N-Methylated 2,4,6-Tri(4-pyridyl)-1,3,5-triazine. *Cryst. Growth Des.* **2017**, *17* (7), 3588−3591.
(15) Li, W.; Wang, Z.; Deschler, F.; Gao, S.; Friend, R. H.; Cheetham, A. K. Chemically diverse and multifunctional hybrid organic−inorganic perovskites. *Nat. Rev. Mater.* **2017**, *2* (3), 16099.
(16) Li, S. L.; Zhang, X. M. Cu3I7 trimer and Cu_4I_8 tetramer based cuprous iodide polymorphs for efficient photocatalysis and luminescent sensing: unveiling possible hierarchical assembly mechanism. *Inorg. Chem.* **2014**, *53* (16), 8376−8383.
(17) Yang, K.; Li, S. L.; Zhang, F. Q.; Zhang, X. M. Simultaneous Luminescent Thermochromism, Vapochromism, Solvatochromism, and Mechanochromism in a C3-Symmetric Cubane $[Cu_4I_4P_4]$ Cluster without Cu-Cu Interaction. *Inorg. Chem.* **2016**, *55* (15), 7323−7325.
(18) Yu, T. L.; Wu, G. X.; Xue, M.; Wang, Z. H.; Fu, Y. L. Five monocyclic pyridinium derivative based halo-argentate/cuprate hybrids or iodide salts: influence of composition on photochromic behaviors. *Dalton Trans* **2018**, *47* (35), 12172−12180.
(19) Qiao, Y.; Hao, P.; Fu, Y. Symmetrically Related Construction and Optical Properties of Two Noncentrosymmetric 3D Iodides of $d^{(10)}$ Cation ($Cu^{(+)}$, $Ag^{(+)}$) Based on the N-Benzylpyridinium and Its Supramolecular Interactions. *Inorg. Chem.* **2015**, *54* (17), 8705−10.
(20) Yue, C. Y.; Lei, X. W.; Han, Y. F.; Lu, X. X.; Tian, Y. W.; Xu, J.; Liu, X. F.; Xu, X. Transition-Metal-Complex Cationic Dyes Photosensitive to Two Types of 2D Layered Silver Bromides with Visible-Light-Driven Photocatalytic Properties. *Inorg. Chem.* **2016**, *55* (23), 12193−12203.
(21) Yue, C. Y.; Yue, Y. D.; Sun, H. X.; Li, D. Y.; Lin, N.; Wang, X. M.; Jin, Y. X.; Dong, Y. H.; Jing, Z. H.; Lei, X. W. Transition metal complex dye-sensitized 3D iodoplumbates: syntheses, structures and photoelectric properties. *Chem. Commun.* **2019**, *55* (48), 6874−6877.
(22) Yue, C. Y.; Hu, B.; Lei, X. W.; Li, R. Q.; Mi, F. Q.; Gao, H.; Li, Y.; Wu, F.; Wang, C. L.; Lin, N. Novel Three-Dimensional Semiconducting Materials Based on Hybrid d(10) Transition Metal Halogenides as Visible Light-Driven Photocatalysts. *Inorg. Chem.* **2017**, *56* (18), 10962−10970.
(23) Lei, X. W.; Yue, C. Y.; Wei, J. C.; Li, R. Q.; Mi, F. Q.; Li, Y.; Gao, L.; Liu, Q. X. Novel 3D Semiconducting Open-Frameworks based on Cuprous Bromides with Visible Light Driven Photocatalytic Properties. *Chem. - Eur. J.* **2017**, *23* (58), 14547−14553.
(24) Lei, X.-W.; Yue, C.-Y.; Zhao, J.-Q.; Han, Y.-F.; Yang, J.-T.; Meng, R.-R.; Gao, C.-S.; Ding, H.; Wang, C.-Y.; Chen, W.-D. Low-Dimensional Hybrid Cuprous Halides Directed by Transition Metal Complex: Syntheses, Crystal Structures, and Photocatalytic Properties. *Cryst. Growth Des.* **2015**, *15* (11), 5416−5426.
(25) Leng, K.; Abdelwahab, I.; Verzhbitskiy, I.; Telychko, M.; Chu, L.; Fu, W.; Chi, X.; Guo, N.; Chen, Z.; Chen, Z.; Zhang, C.; Xu, Q. H.; Lu, J.; Chhowalla, M.; Eda, G.; Loh, K. P. Molecularly thin two-dimensional hybrid perovskites with tunable optoelectronic properties due to reversible surface relaxation. *Nat. Mater.* **2018**, *17* (10), 908−914.
(26) Gratzel, M. The light and shade of perovskite solar cells. *Nat. Mater.* **2014**, *13* (9), 838−842.
(27) Wang, Y.; Zhang, J.; Huang, J.; Zhang, H.; Fu, Z. A lead-iodide based single crystal semiconductor: exploring multi-orientation photoconductive behaviour via intervening isopropyl viologen component between the inorganic $[Pb_2I_6]^{2-}$ wires. *CrystEngComm* **2018**, *20* (15), 2089−2092.
(28) Wang, G. E.; Xu, G.; Wang, M. S.; Cai, L. Z.; Li, W. H.; Guo, G. C. Semiconductive 3-D haloplumbate framework hybrids with high color rendering index white-light emission. *Chem. Sci.* **2015**, *6* (12), 7222−7226.
(29) Lei, X. W.; Yue, C. Y.; Wei, J. C.; Li, R. Q.; Li, Y.; Mi, F. Q. Transition metal complex directed lead bromides with tunable structures and visible light driven photocatalytic properties. *Dalton Trans* **2016**, *45* (48), 19389−19398.
(30) Shen, J. J.; Li, X. X.; Yu, T. L.; Wang, F.; Hao, P. F.; Fu, Y. L. Ultrasensitive Photochromic Iodocuprate(I) Hybrid. *Inorg. Chem.* **2016**, *55* (17), 8271−8273.
(31) Heine, J.; Schmedt auf der Gunne, J.; Dehnen, S. Formation of a strandlike polycatenane of icosahedral cages for reversible one-dimensional encapsulation of guests. *J. Am. Chem. Soc.* **2011**, *133* (26), 10018−10021.
(32) Sun, A. H.; Pan, J.; Han, S. D.; Xue, X. Y.; Wei, Q.; Li, J. H.; Wang, G. M. In Situ Ligand Modification Strategy for the Construction of One-, Two-, and Three-Dimensional Heterometallic Iodides. *Inorg. Chem.* **2017**, *56* (22), 13785−13793.
(33) Wei, Q.; Ge, B. D.; Zhang, J.; Sun, A. H.; Li, J. H.; Han, S. D.; Wang, G. M. Tripyridine-Derivative-Derived Semiconducting Iodo-Argentate/Cuprate Hybrids with Excellent Visible-Light-Induced Photocatalytic Performance. *Chem. - Asian J.* **2019**, *14* (2), 269−277.
(34) Sun, A. H.; Wei, Q.; Fu, A. P.; Han, S. D.; Li, J. H.; Wang, G. M. Syntheses, structures and efficient visible light-driven photocatalytic properties of layered cuprous halides based on two types of building units. *Dalton Trans* **2018**, *47* (20), 6965−6972.

https://dx.doi.org/10.1021/acs.inorgchem.0c03665
Inorg. Chem. 2021, 60, 2105−2111

(35) Blessing, R. H. An empirical correction for absorption anisotropy. *Acta Crystallogr., Sect. A: Found. Crystallogr.* **1995**, *A51*, 33−38.
(36) Sheldrick, G. M. *SHELXTL-97, Program for Solution of Crystal Structures*; University of Göttingen: Göttingen, Germany, 1997.
(37) Sheldrick, G. M. *SHELXS-97, Program for Solution of Crystal Refinement*; University of Göttingen: Göttingen, Germany, 1997.
(38) Sun, S.; Wei, Q.; Huang, Y.; Yuan, F.; Lou, F.; Zhong, D.; Zhang, L.; Lin, Z.; Teng, B. Enhanced growth of Nd^{3+}:$MgGdB_5O_{10}$ laser crystals with intense multi-wavelength emission characteristics. *J. Mater. Chem. C* **2020**, *8* (21), 7104−7112.
(39) Clark, S. J.; Segall, M. D.; Pickard, C. J.; Hasnip, P. J.; Probert, M. J.; Refson, K.; Payne, M. C. First principles methods using CASTEP. *Z. Kristallogr. - Cryst. Mater.* **2005**, *220*, 567−570.
(40) Zhang, W. C.; Liu, X. T.; Li, L. N.; Sun, Z. H.; Han, S. G.; Wu, Z. Y.; Luo, J. H. Triiodide-Induced Band-Edge Reconstruction of a Lead-Free Perovskite-Derivative Hybrid for Strong Light Absorption. *Chem. Mater.* **2018**, *30* (12), 4081−4088.
(41) Ge, B. D.; Wei, Q.; Sun, A. H.; Lin, C. Y.; Duan, X. F.; Li, J. H.; Wang, G. M. A 3D Iodoplumbate Semiconducting Open Framework with Visible-light-induced Photocatalytic Performance. *Chem. - Asian J.* **2019**, *14* (12), 2086−2090.
(42) Gao, Y.; Li, S.; Li, Y.; Yao, L.; Zhang, H. Accelerated photocatalytic degradation of organic pollutant over metal-organic framework MIL-53(Fe) under visible LED light mediated by persulfate. *Appl. Catal., B* **2017**, *202*, 165−174.
(43) Zhang, T.; Lin, W. Metal−organic frameworks for artificial photosynthesis and photocatalysis. *Chem. Soc. Rev.* **2014**, *43* (16), 5982−5993.
(44) Du, Y.; Ma, W.; Liu, P.; Zou, B.; Ma, J. Magnetic $CoFe_2O_4$ nanoparticles supported on titanate nanotubes ($CoFe_2O_4$/TNTs) as a novel heterogeneous catalyst for peroxymonosulfate activation and degradation of organic pollutants. *J. Hazard. Mater.* **2016**, *308*, 58−66.
(45) Lin, S.; Hao, P.; Shen, J.; Fu, Y. Hierarchically responsive and photochromic imidazopyridazinium iodoargentate hybrid materials. *Dyes Pigm.* **2018**, *159*, 457−463.
(46) Bresolin, B.-M.; Park, Y.; Bahnemann, D. W. Recent Progresses on Metal Halide Perovskite-Based Material as Potential Photocatalyst. *Catalysts* **2020**, *10* (6), 709.
(47) Shen, J.; Zhang, C.; Yu, T.; An, L.; Fu, Y. Structural and Functional Modulation of Five 4-Cyanopyridinium Iodoargentates Built Up from Cubane-like Ag_4I_4 Nodes. *Cryst. Growth Des.* **2014**, *14* (12), 6337−6342.
(48) Jiang, X.-F.; Wei, Q.; Ge, B.-D.; Fu, A.-P.; Li, J.-H.; Wang, G.-M. Optical and photocatalytic properties of conjugated-organic-templates derived semiconducting iodocuprates hybrids. *Opt. Mater.* **2020**, *109*, 110376.

https://dx.doi.org/10.1021/acs.inorgchem.0c03665
Inorg. Chem. 2021, 60, 2105−2111